Active nematic response to a deformable body or boundary: Elastic deformations and anchoring-induced flow

Thomas G. J. Chandler [*] and Saverio E. Spagnolie [†]
Department of Mathematics, University of Wisconsin–Madison, Madison, Wisconsin 53706, USA

(Received 23 September 2024; revised 15 April 2025; accepted 30 May 2025; published 13 June 2025)

A body immersed in a nematic liquid crystal disturbs the fluid's preferred molecular configuration and increases its stored elastic energy. In an active nematic, the fluid components also generate a stress in the bulk fluid. By introducing either an immersed body or boundary, a large scale flow can be triggered due to anchoring boundary conditions alone—a global pressure built by active stresses at equilibrium is instantly released everywhere. The fluid then imposes viscous, elastic, and active stresses on such surfaces which, if compliant, may result in a surface deformation. We study the deformations and stresses of a linearly elastic body placed in an active nematic in two dimensions. Using complex variable techniques, exact expressions for the fluid flow, director field, surface tractions, and body deformation are derived. Qualitative differences between elastic and active stress-driven deformations are identified, depending on an active Ericksen number, anchoring conditions, and body material properties, thereby suggesting a new method for measuring mechanical stresses in active anisotropic environments. Flow profiles, external confinement, and anchoring-induced stirring are also addressed.

DOI: 10.1103/x8y2-tw4c

I. INTRODUCTION

The eukaryotic cell is host to a wide variety of deformable organelles, from the nucleus to mitochondria [1–6]. These organelles reside in complex environments which can be anisotropic [7,8], and experience mechanical stresses due to actively driven cytoplasmic flows [9–15]. The cell membrane itself is also deformable, and its morphology is commonly influenced by internal processes. For instance, active anisotropic stresses are of functional importance in cytoskeletal remodeling of the nucleus and chromatin configurations [16–20], in the metaphase spindle [21–23], and in numerous other aspects of tissue morphogenesis [24–26]. On a larger length scale, active systems like bacterial swarms and biofilms also exhibit anisotropy, among other complex rheological properties [27–31].

Even when free of bodies, actively driven anisotropic flows exhibit very rich and complex dynamics [32–36]. Stability [34,37–43], topology [44], pattern formation [45–47], and mixing [48,49] have seen substantial theoretical treatment. Confinement introduces an additional length scale, which can affect the emergent spatial structure [50,51]. Strong active nematic stresses can also change the shape of deformable confining surfaces [52–59], and can play a prominent role in directing the motility of cells [60,61] and active droplets [62–65].

When an active nematic contains an immersed body, or inclusion, additional elastic stresses are immediately introduced. In passive systems, these stresses result in intricate and beautiful textures [66–68], and can be used to measure cell material properties [69,70]. In active systems, fluid elasticity and anisotropy can redirect the emergent flows, leading to complex body dynamics. Recent examples include an investigation of the biased rotation of gearlike bodies [71,72], complex droplet trajectories [73,74], and transitions from fixed point to limit cycle to chaotic dynamics of a circular disk [75]. How body deformability affects and is affected by such an active environment remains largely unexplored.

In this paper, we study an active nematic fluid based on the Ericksen–Leslie theory [36,76–79] with a soft internal or external boundary in two dimensions. Complex variable techniques yield exact analytical representations for the director field, velocity field, and boundary deformation. Elastic deformations of bounding surfaces are known to relieve the elastic energy stored in the bulk LC phase [80]. Here, we show that active stresses can compete and eventually dominate this balance, resulting in distinct geometric signals. In addition, we show that a spontaneous stirring flow with a unique plume structure may be induced with a change in surface anchoring boundary conditions alone, due to a global pressure release.

II. ACTIVE NEMATIC FLOWS

Active nematic liquid crystals (LCs) can be described by their locally averaged molecular orientation (i.e., the director field) $\boldsymbol{n}(\boldsymbol{x}, t)$ and fluid velocity $\boldsymbol{u}(\boldsymbol{x}, t)$, with spatial position $\boldsymbol{x}$, time t, and $|\boldsymbol{n}| = 1$. The director field, $\boldsymbol{n}$, evolves due to

[*]Contact author: tgchandler@wisc.edu
[†]Contact author: spagnolie@wisc.edu

Published by the American Physical Society under the terms of the Creative Commons Attribution 4.0 International license. Further distribution of this work must maintain attribution to the author(s) and the published article's title, journal citation, and DOI.

gradients in the velocity field, with strain-rate tensor $E_{ij} = (\partial_i u_j + \partial_j u_i)/2$ and vorticity tensor $\Omega_{ij} = (\partial_i u_j - \partial_j u_i)/2$, and a relaxation toward equilibrium under the action of the molecular field, $\boldsymbol{H} = -\delta\mathcal{F}/\delta\boldsymbol{n}$, where $\mathcal{F}$ is the free energy density. In the one-constant approximation, $\mathcal{F} = K\|\nabla\boldsymbol{n}\|^2/2$ and so $\boldsymbol{H} = K\nabla^2\boldsymbol{n}$, for the single (Frank) elastic constant K [77]. Together,

$$(\partial_t + \boldsymbol{u}\cdot\nabla)\boldsymbol{n} = \boldsymbol{n}\cdot\boldsymbol{\Omega} + \lambda\boldsymbol{n}\cdot\mathbf{E}\cdot(\mathbf{I} - \boldsymbol{nn}) + \boldsymbol{h}/\gamma, \quad (1)$$

with γ the rotational viscosity, λ the tumbling/reactive parameter, and $\boldsymbol{h} = (\mathbf{I} - \boldsymbol{nn})\cdot\boldsymbol{H}$ the transverse part of the molecular field, where $\boldsymbol{nn}$ is a dyadic product [76–78,80]. Momentum and mass conservation, under the assumptions of incompressibility and zero Reynolds number flow,[1] are given by

$$\nabla\cdot(\boldsymbol{\sigma}^e + \boldsymbol{\sigma}^v + \boldsymbol{\sigma}^a - p\mathbf{I}) = \mathbf{0}, \quad (2a)$$

$$\text{and} \quad \nabla\cdot\boldsymbol{u} = 0, \quad (2b)$$

respectively, for $\nabla\cdot\boldsymbol{\sigma} := \partial_i\sigma_{ij}$, pressure p, and elastic, viscous, and active stress tensors

$$\boldsymbol{\sigma}^e = \frac{K}{2}\|\nabla\boldsymbol{n}\|^2\mathbf{I} - K\nabla\boldsymbol{n}\cdot\nabla\boldsymbol{n}^T - \frac{1}{2}(\boldsymbol{nh} - \boldsymbol{hn}) - \frac{\lambda}{2}(\boldsymbol{nh} + \boldsymbol{hn}), \quad (3a)$$

$$\boldsymbol{\sigma}^v = 2\mu\mathbf{E} + \mu_1(\boldsymbol{n}\cdot\mathbf{E}\cdot\boldsymbol{n})\boldsymbol{nn} + \mu_2(\boldsymbol{n}\mathbf{E}\cdot\boldsymbol{n} + \boldsymbol{n}\cdot\mathbf{E}\boldsymbol{n}), \quad (3b)$$

$$\boldsymbol{\sigma}^a = 2\alpha\boldsymbol{nn}, \quad (3c)$$

respectively. Here, μ is the solvent viscosity, μ_1 and μ_2 are anistropic viscosities, and α is the activity strength, which can describe both extensile ($\alpha < 0$) and contractile ($\alpha > 0$) activity [36,79,81] (see [82]). Note the convention taken for the divergence, which is important since $\boldsymbol{\sigma}^e$ is not symmetric.

The system is made dimensionless by scaling upon an intrinsic length scale L (e.g., the size of an immersed body), velocity scale U (to be defined), and stress scale K/L^2. The system is then characterized by the dimensionless Ericksen number, activity strength, and viscosity ratios [82]:

$$\mathrm{Er} := \frac{\mu UL}{K}, \quad A := \frac{\alpha L}{\mu U}, \quad \gamma' := \frac{\gamma}{\mu}, \quad \mu_j' := \frac{\mu_j}{\mu}. \quad (4a\text{–}d)$$

For small rotational Ericksen numbers, $\gamma'\mathrm{Er} \ll 1$, the fluid flow does not affect the director field, and at leading order from (1) we have

$$\boldsymbol{h} = (\mathbf{I} - \boldsymbol{nn})\cdot\nabla^2\boldsymbol{n} = \mathbf{0}. \quad (5)$$

Further, assuming small viscosity ratios, $\gamma', \mu_i' \ll 1$, Eq. (2a) yields

$$-\nabla p + \nabla^2\boldsymbol{u} + 2A\nabla\cdot(\boldsymbol{nn}) = \mathbf{0}. \quad (6)$$

In the examples presented in this paper, the fluid flow is induced by activity alone; thus, the velocity scale is set by the activity strength, $U = |\alpha|L/\mu$, and the assumption of a small Ericksen number is equivalent to assuming weak activity, $\gamma'\mathrm{Er} = |\alpha|\gamma L^2/(\mu K) \ll 1$.[2]

A. Two-dimensional active nematics

In 2D, the director field can be described by an angle field $\theta(x, y) \in [0, \pi)$ such that $\boldsymbol{n} = (\cos\theta, \sin\theta)$, and a streamfunction $\psi(x, y)$ can be introduced such that $\boldsymbol{u} = (\partial_y\psi, -\partial_x\psi)$. The director field, governed by $\boldsymbol{h} = \mathbf{0}$, reduces to Laplace's equation for θ, while the momentum equation (6) is equivalent to Poisson's equation for the scalar vorticity, $\omega = -\nabla^2\psi$:

$$\nabla^2\theta = 0, \quad (7a)$$

$$\nabla^2\omega = A[2\partial_{yx}\cos(2\theta) + (\partial_{yy} - \partial_{xx})\sin(2\theta)]. \quad (7b)$$

Here, we absorb the isotropic parts of the stress tensors into the pressure by taking $p \mapsto p + A$. The leading-order, dimensionless, traceless stress tensors are denoted with hats:

$$\hat{\boldsymbol{\sigma}}^e = \tfrac{1}{2}|\nabla\theta|^2\mathbf{I} - \nabla\theta\nabla\theta, \quad (8a)$$

$$\hat{\boldsymbol{\sigma}}^v = \nabla\boldsymbol{u} + \nabla\boldsymbol{u}^T, \quad (8b)$$

$$\hat{\boldsymbol{\sigma}}^a = 2\boldsymbol{nn} - \mathbf{I}, \quad (8c)$$

giving the dimensionless (bulk) stress tensor $\boldsymbol{\sigma} = \hat{\boldsymbol{\sigma}}^e + \mathrm{Er}(\hat{\boldsymbol{\sigma}}^v + A\hat{\boldsymbol{\sigma}}^a - p\mathbf{I})$.

At any boundaries, we assume the fluid velocity vanishes and the director field relaxes locally toward a preferred angle $\theta_0(s)$ due to surface anchoring of strength W (i.e., Rapini–Papoular anchoring [83]):

$$\partial_s\psi = \partial_\nu\psi = 0 \quad (9a)$$

$$\text{and} \quad \partial_\nu\theta = \frac{w}{2}\sin[2(\theta - \theta_0)], \quad (9b)$$

for the anticlockwise arclength derivative $\partial_s = \hat{\boldsymbol{s}}\cdot\nabla$, normal derivative pointing into the LC $\partial_\nu = \hat{\boldsymbol{\nu}}\cdot\nabla$, and the dimensionless anchoring strength $w := WL/K$.

With $z = x + \mathrm{i}y$ and $\bar{z} = x - \mathrm{i}y$ its complex conjugate, the system may be written in complex variables as

$$\partial_{z\bar{z}}\theta = 0 \quad (10a)$$

$$\text{and} \quad \partial_{\bar{z}}(p - \mathrm{i}\omega) = A\partial_z e^{2\mathrm{i}\theta}, \quad (10b)$$

with vorticity $\omega = -4\partial_{z\bar{z}}\psi$ and velocity $\boldsymbol{u} = (u, v)$, given by $u - \mathrm{i}v = 2\mathrm{i}\partial_z\psi$. Integrating (10) yields

$$\theta = -\arg f'(z) \quad (11a)$$

$$\text{and} \quad p - \mathrm{i}\omega = A\partial_z[g(z) + \overline{f(z)}/f'(z)], \quad (11b)$$

for some locally holomorphic functions f and g [84]. We assume the LC does not contain any topological defects, so f is nonzero and singularity free inside the LC, though this assumption can be relaxed [85,86]. Inserting the imaginary

[1] The Reynolds number is defined as $\mathrm{Re} = \rho|\alpha|L^2/\mu^2$, with ρ the fluid density, and other terms defined above.

[2] In 2D incompressible flows, a general μ_2 can actually be absorbed into the isotropic viscosity by taking $\mu \mapsto \mu - \mu_2/2$.

part of (11b) into $\partial_{z\bar{z}}\psi = -\omega/4$ and integrating yields

$$\psi = \frac{A}{4}\,\mathrm{Im}\left[\bar{z}g(z) + h(z) + \overline{\int f(z)\,dz}\,/f'(z)\right], \tag{12}$$

for another locally holomorphic function h. The first two terms in (12) correspond to the well-known form of a biharmonic function with Goursat functions h and g [87], while the last term accounts for the active forcing.

Analytical solutions for the director and velocity fields are obtained, provided that functions f, g, and h, which are locally holomorphic within the LC and satisfy the boundary conditions in (9), may be found. The problem for f derived here is equivalent to the potential problem explored in Refs. [88,89] for a passive LC, but g and h depend on activity.

B. Anchoring-controlled flows

As an example, consider a cylinder of radius L of infinite extent immersed in a weakly-active nematic LC. In the far field, we assume the LC is aligned horizontally in a direction orthogonal to the cylinder's long axis and the fluid velocity vanishes. The LC is assumed to be tangentially anchored to the body with finite strength, i.e., (9b) with $\theta_0 = \arg(\mathrm{i}z)$ mod π on $|z| = 1$. Without the body, the system sits at an equilibrium, with $\boldsymbol{n} = \hat{\boldsymbol{x}}$ and $\boldsymbol{u} = \boldsymbol{0}$, and the active stress is absorbed by the pressure.

To find the activity-induced flow, we first determine the LC director angle $\theta = -\arg f'$. Here, the potential $f(z)$ must be locally holomorphic in $1 < |z| < \infty$ and satisfy the finite anchoring condition on $|z| = 1$, and $f(z) \sim z$ as $|z| \to \infty$. The solution to this problem is

$$\theta = -\arg f'(z) = -\arg(1 - \rho^2/z^2), \tag{13}$$

where $\rho(w) := (\sqrt{1 + 4/w^2} - 2/w)^{1/2}$ is an effective radius [88]. The corresponding director lines (which lay parallel to $\boldsymbol{n}$) are plotted in Fig. 1(a) for $w = 10$. Meanwhile, the Goursat functions $h(z)$ and $g(z)$ must be locally holomorphic in $1 < |z| < \infty$ and yield a fluid velocity that vanishes on $|z| = 1$ and as $|z| \to \infty$. This ultimately yields the streamfunction (see [82]):

$$\psi = \frac{A\rho^2}{8}\,\mathrm{Im}\left[\frac{(|z|^2 - 1)^2}{z^2(z^2 - \rho^2)} + \frac{1 - |z|^2 + 2\log|z|}{(z^2 - \rho^2)/(2\rho^2)}\right]. \tag{14}$$

The corresponding flow is shown in Figs. 1(b) and 1(c) for $w = 1$ and $w = 10$, with $A = -1$ (i.e., extensile activity).

A prominent feature of the induced flow is a plume extending symmetrically to both the left and right of the cylinder [see Figs. 1(b) and 1(c)]. Far from the body,

$$u + \mathrm{i}v = -2\mathrm{i}\partial_{\bar{z}}\psi \sim [\rho^2\cos(2\vartheta) - \cos(4\vartheta)]\frac{A\rho^2 e^{\mathrm{i}\vartheta}}{2|z|}, \tag{15}$$

as $|z| \to \infty$, for $\vartheta = \arg z$. This far-field flow behavior is critically dependent on the effective radius $\rho(w)$, and hence the anchoring strength w. The plume angle, thus, decreases from $\pi/4$ to 0 as the anchoring strength w is increased from 0 to ∞, while the plume speed is largest at $w = 8/3$. The velocity field does not appear as a dipole or stresslet in the far field, but the sum of a dipole and a quadrupole—the mere presence of the body initiates additional flow far away due to the distributed active stress, leading to bulk flow release. This also demonstrates that a body with nontrivial anchoring conditions is sufficient to induce a large scale flow through its presence alone.

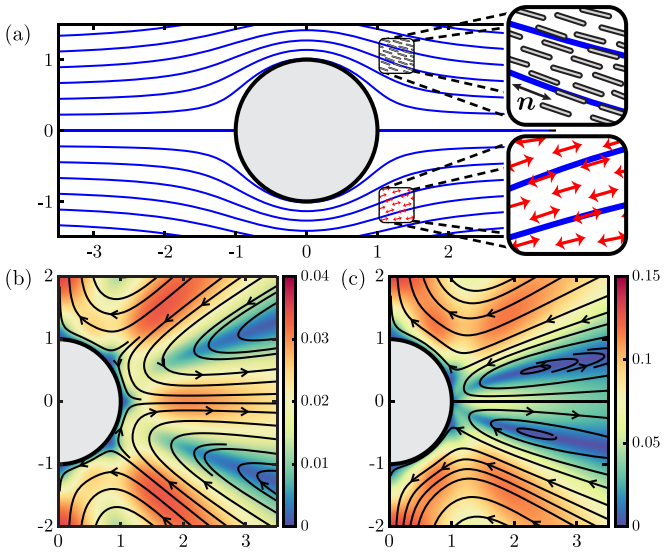


FIG. 1. The activity-induced flow of a 2D nematic LC outside a cylinder for $A = -1$ (i.e., extensile activity). (a) The director lines for $w = 10$ are shown as blue curves. (b), (c) The activity-induced velocity field is shown for (b) $w = 1$ and (c) $w = 10$. The black arrows show the flow direction and the color denotes the fluid speed, $\sqrt{u^2 + v^2}$. Contractile activity with $A = 1$ corresponds to flipping the flow direction.

III. SURFACE TRACTIONS AND SOFT BOUNDARIES

Stresses due to passive LC elasticity, actively driven viscous flow, and direct activity all contribute to surface forcing. The LC introduces a surface traction $\boldsymbol{t}^e = \hat{\boldsymbol{\nu}} \cdot \hat{\boldsymbol{\sigma}}^e + \partial_s \boldsymbol{t}^s$, where $\hat{\boldsymbol{\sigma}}^e$ is the Ericksen elastic stress tensor given in (8), and

$$\boldsymbol{t}^s = \frac{w}{2}\sin^2(\theta - \theta_0)\hat{\boldsymbol{s}} + \frac{w}{2}\sin[2(\theta - \theta_0)]\hat{\boldsymbol{\nu}} \tag{16}$$

is a surface stress vector associated with finite surface anchoring [80]. Activity, meanwhile, produces a surface traction $\boldsymbol{t}^a = \mathrm{Er}\,\hat{\boldsymbol{\nu}} \cdot (\hat{\boldsymbol{\sigma}}^v + A\hat{\boldsymbol{\sigma}}^a - p\mathbf{I})$ for the (traceless) viscous and active stress tensors $\hat{\boldsymbol{\sigma}}^v$ and $\hat{\boldsymbol{\sigma}}^a$ given in (8).

If a boundary is soft, it will generally be deformed by the surface tractions above. As a first step toward understanding more complex materials, we assume the boundary is part of an isotropic solid that deforms according to plane stress/strain in the framework of linear elasticity, with shear modulus μ_s and Poisson's ratio ν [90,91]. At equilibrium, the elastic solid can be described by an Airy-stress function, $\mathcal{A}(x, y)$, which satisfies the biharmonic equation, $\nabla^4\mathcal{A} = 0$. We can, thus, write

$$\mathcal{A} = \mathrm{Im}[\bar{z}G(z) + H(z)], \tag{17}$$

for two (new) Goursat functions, G and H, that are locally holomorphic within the solid (but not necessarily the LC), analogous to g and h in (12) [90]. These Goursat functions

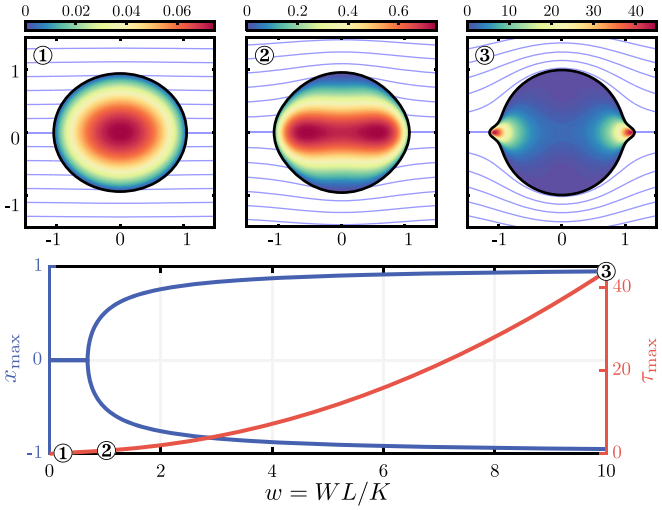


FIG. 2. (Top) Deformation of a soft cylinder immersed in a passive nematic LC with $A\mathrm{Er} = 0$, $M/w = 5$, $\kappa = 5/3$, and dimensionless anchoring strengths ① $w = 0.1$, ② $w = 1$, and ③ $w = 10$. Color indicates the maximum shear stress, $\tau = \sqrt{(\Sigma_{11} - \Sigma_{22})^2/4 + \Sigma_{12}^2}$, within the cylinder and the blue curves are director lines. (Bottom) The positions, $(x_{\max}, 0)$, and value, $\tau_{\max} = \max_x \tau$, of the largest maximum shear stress plotted as a function of w.

yield the symmetric stress tensor within the solid, Σ_{ij}, via the Kolosov–Muskhelishvili formulas,

$$\Sigma_{11} - \Sigma_{22} - 2\mathrm{i}\Sigma_{12} = 2\mathrm{i}\bar{z}G''(z) + 2\mathrm{i}H''(z) \quad (18a)$$

$$\text{and} \quad \Sigma_{11} + \Sigma_{22} = 4\,\mathrm{Im}\,G'(z), \quad (18b)$$

and the solid displacement, (U, V), can be expressed as

$$2M(U - \mathrm{i}V) = \mathrm{i}\kappa\overline{G(z)} + \mathrm{i}\bar{z}G'(z) + \mathrm{i}H'(z), \quad (19)$$

up to an arbitrary body displacement and rotation, for the dimensionless elastic modulus $M := \mu_s L^2/K$ and $\kappa = (3 - 4\nu)$ or $(3 - \nu)/(1 + \nu)$, when assuming plane strain or plane stress, respectively.

Stress balance at the LC-solid interface, $\hat{\boldsymbol{\nu}} \cdot \boldsymbol{\Sigma} + \boldsymbol{t}^e + \boldsymbol{t}^a = \boldsymbol{0}$, yields the boundary conditions for G and H:

$$\partial_s[\bar{z}G'(z) - \overline{G(z)} + H'(z)] = \left(t_x^e + t_x^a\right) - \mathrm{i}\left(t_y^a + t_y^e\right). \quad (20)$$

A. Activity-controlled deformations

Returning to the example of a unit cylinder with tangential anchoring, the director angle (13) and streamfunction (14) yield analytic expressions for the elastic traction, $t_x^e + \mathrm{i}t_y^e$, and activity-induced traction, $t_x^a + \mathrm{i}t_y^a = A\mathrm{Er}(1/z - \rho^2 z)$. The cylinder is now assumed to be deformable, and so, we seek the Airy stress (17). Here, the Goursat functions $G(z)$ and $H(z)$ must be locally holomorphic in $|z| < 1$ and satisfy (20) on $|z| = 1$; the solution is provided in [82].

Without activity ($A = 0$), boundary deformations help to reduce the elastic energy stored in the bulk LC [80]. Figure 2 shows the LC configurations and body deformations for three different anchoring strengths and $\kappa = 5/3$ (i.e., an incompressible cylinder, $\nu = 1/2$, under plane stress). For large anchoring strengths, $w \gg 1$, most of the LC energy is stored local to the left and right poles of the cylinder, with a singular energy emerging in the case of strong (infinite) anchoring ($w = \infty$) due to the appearance of two -1 Boojum topological defects at $z = \pm 1$ [88,92]. This localized energy within the LC results in large localized surface tractions as $w \to \infty$: $t_x^e + \mathrm{i}t_y^e = \mathcal{O}(w^2)$ when $z \pm 1 = \mathcal{O}(1/w)$, and $t_x^e + \mathrm{i}t_y^e = \mathcal{O}(1)$ otherwise. This, in turn, leads to large localized deformations; in particular, we find that

$$U + \mathrm{i}V \sim \frac{3w}{8M}[\mathcal{U}(1 - z) - \mathcal{U}(1 + z)], \quad (21)$$

as $w \to \infty$, where

$$\mathcal{U}(Z/w) = \frac{\kappa}{1 + Z} + \frac{1}{1 + \bar{Z}} + \frac{Z + \bar{Z}}{(1 + \bar{Z})^2} \quad (22)$$

corresponds to a deformation that is only apparent when $z \pm 1 = \mathcal{O}(1/w)$. As the anchoring strength decreases, stress is no longer concentrated at the poles and the maximum shear stress $\tau(x, y) = \sqrt{(\Sigma_{11} - \Sigma_{22})^2/4 + \Sigma_{12}^2}$ (a common indicator of mechanical failure [91]) is greatest at $(\pm x_{\max}, 0)$, where $x_{\max}$ decreases from 1 when $w = \infty$, to 0 when $w \leqslant 24/35$, as shown in Fig. 2.

In an active nematic ($A \neq 0$), the activity leads to an additional deformation:

$$U + \mathrm{i}V = U^e + \mathrm{i}V^e + \frac{A\mathrm{Er}}{4M}[(1 - \kappa)\rho^2 z + 2\bar{z}], \quad (23)$$

where (U^e, V^e) is the deformation of a cylinder immersed in a passive LC. As this addition is proportional to the activity strength, A, activity can act with or against the elastic effects of the LC, depending on if it is extensile ($A < 0$) or contractile ($A > 0$). In particular, the aspect ratio, $\mathcal{A}_R$, of the deformed cylinder is given by

$$\mathcal{A}_R \sim 1 + U\big|_{z=1} - V\big|_{z=i} = 1 + \frac{A\mathrm{Er} - \mathcal{W}}{M}, \quad (24)$$

where

$$\mathcal{W} = \frac{3\kappa}{2\rho}(\mathrm{arctanh}\,\rho - \arctan\rho) - \frac{3w}{8}(1 + \kappa). \quad (25)$$

Thus, if $A\mathrm{Er} > \mathcal{W}$ (which includes passive LCs since $\mathcal{W} < 0$), the deformed shape is elongated with the x axis (i.e., the preferred axis of the LC). While, if $A\mathrm{Er} < \mathcal{W}$, the shape is elongated with the y axis (i.e., perpendicular to the preferred axis). The aspect ratio is one at the critical value $A\mathrm{Er} = \mathcal{W}$, see Fig. 3. Therefore, contractile activity ($A > 0$), in this setting, always leads to parallel elongation, while extensile activity ($A < 0$) yields perpendicular elongation, as long as the activity is sufficiently strong.

B. Bounded domains and spontaneous stirring

The fluid flow triggered by the presence of a boundary may also be advantageous in interior domains like biological cells—settings in which a distribution of molecules, such as nutrients, chemicals, or oxygen, benefit the system's function [93–96]. Consider an active nematic LC bounded inside and (weakly) tangentially anchored to a cylinder with anchoring strength w. Here, the director angle of the LC can be written as $\theta = \arg(1 - \rho^2 z^2)$, for the effective radius introduced in the external problem, $\rho(w) = (\sqrt{1 + 4/w^2} - 2/w)^{1/2}$, while the

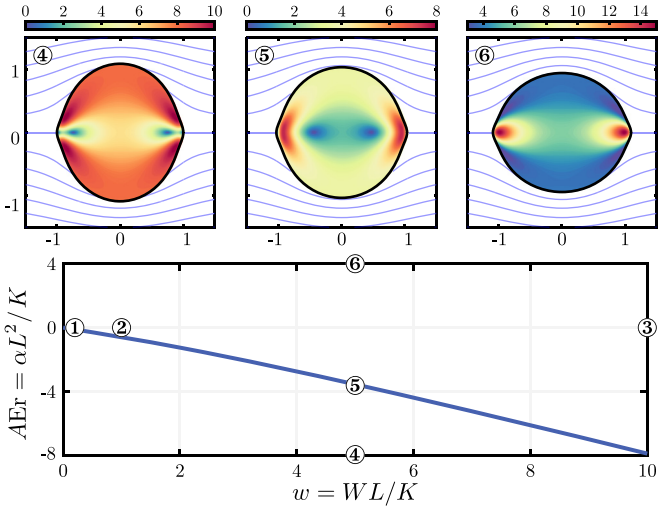


FIG. 3. (Top) Deformation of a soft cylinder immersed in an active nematic LC with $w = 5$, $M = 50$, $\kappa = 5/3$, and ④ $A\mathrm{Er} = -8 < \mathcal{W}$ (extensile), ⑤ $A\mathrm{Er} = \mathcal{W} \approx -3.55$ (extensile), and ⑥ $A\mathrm{Er} = 4 > \mathcal{W}$ (contractile). Color indicates the maximal shear stress, $\sqrt{(\Sigma_{11} - \Sigma_{22})^2/4 + \Sigma_{12}^2}$, within the cylinder and the blue curves are director lines. (Bottom) The critical active Ericksen number, $A\mathrm{Er} = \mathcal{W}$, at which the deformed cylinder has aspect ratio one, plotted as a function of w for $\kappa = 5/3$. The points ①–③ correspond to the configurations shown in Fig. 2.

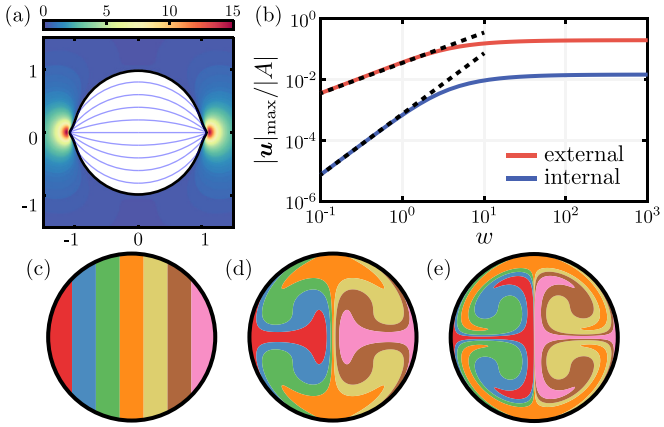


FIG. 4. (a) Deformation of a soft cylinder enclosing a passive nematic LC with $A\mathrm{Er} = 0$, $w = 10$, $M = 50$, and $\kappa = 5/3$. Color delineates the maximum shear stress, $\sqrt{(\Sigma_{11} - \Sigma_{22})^2/4 + \Sigma_{12}^2}$, within the solid, and the blue curves are director lines. (b) Plot of the maximum fluid speed, $|\boldsymbol{u}|_{\max} = \max_{\boldsymbol{x}} \sqrt{u^2 + v^2}$, as a function of w for the LC external and internal to a cylinder. The asymptotic behaviors as $w \to 0$ are shown as black dashed lines. (c)–(e) Snapshots at times (c) $t = 0$, (d) $t = 100/|A|$, and (e) $t = 200/|A|$ of colored fluid particles transported due to extensile activity inside the cylinder for $w = 10$.

flow can be expressed in terms of a streamfunction (see [82]):

$$\psi = \frac{A}{8}(|z|^2 - 1)\,\mathrm{Im}\left[\frac{1-\rho z}{z^2}\log(1-\rho z) + \frac{1+\rho z}{z^2}\log(1+\rho z)\right]. \tag{26}$$

Figure 4(a) shows the director lines inside a cylinder that has deformed according to linear elasticity [82]. The final deformed shape resembles a tactoid [97], with a localized deformation at the left and right poles occurring for large anchoring strengths due to the appearance of two +1 aster defects when $w = \infty$. The deformed shape is dependent on the active Ericksen number, $A\mathrm{Er}$, with extensile activity ($A < 0$) leading to parallel elongation and sufficient contractile activity ($A < 0$) yielding perpendicular elongation [82]—opposite to the dependence on the activity strength in the external problem.

Figures 4(c)–4(e) show stirring induced by extensile activity. Varying the activity and anchoring strength affects the rate of stirring. The maximum fluid speed, $|\boldsymbol{u}|_{\max}$, is plotted as a function of anchoring strength in Fig. 4(b), for both the external and internal problems. The speeds plateau for large anchoring strengths, and decrease according to $|\boldsymbol{u}|_{\max} \sim 2|A|w/(25\sqrt{5})$ and $|\boldsymbol{u}|_{\max} \sim |A|w^2/(600\sqrt{5})$ as $w \to 0$, for the external and internal problem, respectively. The extent to which this stirring flow is mixing is an interesting but separate question [98]. Mixing is notoriously challenging in highly viscous flows and in confined geometries [99], but is likely promoted by a wide spatial distribution of active stress [48,49].

IV. CONCLUSIONS AND DISCUSSIONS

We have shown that the configurations and dynamics of an active nematic can be affected dramatically by the mere presence of a boundary, for any nontrivial anchoring strength. It suggests that energy bound in a uniform active nematic can be released as a large scale flow due to a localized inclusion alone.

The spontaneous flow that arises is characterized by unique plumes whose structure is anchoring strength dependent. The body may then deform in response to this anisotropic, viscoelastic flow, in a generally localized manner near (virtual) topological defects. Such flows can also produce a spontaneous stirring, and likely mixing, of the environment. The associated symmetry breaking can lead to cell or droplet division and motility [100–102]. Looking to the horizon, biological cells are host to a multitude of active anisotropic networks. Can such fluids be triggered into motion solely by the passive anchoring conditions on an arriving organelle? This mechanism could offer an energy-efficient way to generate precisely timed mixing flows within the cellular environment.

New experiments on the shapes and dynamics of deformable inclusions in active nematics is needed. Testable hypotheses include the differential direction of elongation, which may be tuned by varying either the activity strength (e.g., by changing the density of molecular motors [23]) or by changing the body stiffness. With sufficient perpendicular elongation due to strong extensile activity, as in the top left panel of Fig. 3, body rotation may also ensue to reduce the bulk elastic energy. We thus predict that a diverse zoology of body dynamics will emerge with increasing extensile activity in particular.

Consequences for intracellular form and function are also expected. Taking the metaphase spindle as an

example [22,103], using a length scale $L = 20\,\mu\text{m}$, bulk elastic constant $K = 400\,\text{pN}$ [23], and contractile activity strength $\alpha \sim 35\,\text{pN}/\mu\text{m}^2$ [23,53,104], we find that $A\text{Er} \approx 35$. Balancing against surface tension, comparable parameters can provide the spindle's characteristic shape [23,53]. Such elastic and activity-induced stresses would both stretch an immersed body in the direction parallel to the background director field. These mechanics would seem to be of additional service in the splitting of sister chromatids, which separate and are pulled toward the two spindle poles during anaphase A [105,106]. Chromosomes can also be repelled in a direction perpendicular to the director in metaphase, due to LC elastic interactions [89,107]. Our results suggest a more complex picture if active stresses are included, which would impose an additional attraction (e.g., from Fig. 1 with oppositely signed flow).

Extensile activity in a related synthetic system, taking $L \approx 200\,\mu\text{m}$, instead has $A\text{Er} \approx -1500$ [35,71,108]. Such a highly extensile suspension is likely to result in large deformations of any soft inclusions in the direction perpendicular to the background director field. This could add to the already complex body dynamics that have been observed in such systems [71].

Future directions will require different machinery. Large deformations will more completely couple the LC configuration and flows, and a finite rotational viscosity will introduce an additional timescale [77,109]. The analytical limits provided herein may still be of use for steering investigations of these more highly nonlinear regimes.

ACKNOWLEDGMENTS

We acknowledge helpful discussions with Nicholas L. Abbott and Ido Lavi. Support for this research was provided by the Office of the Vice Chancellor for Research and Graduate Education with funding from the Wisconsin Alumni Research Foundation.

[1] P. Isermann and J. Lammerding, Nuclear mechanics and mechanotransduction in health and disease, Curr. Biol. **23**, R1113 (2013).

[2] K. Haase, J. K. Macadangdang, C. H. Edrington, C. M. Cuerrier, S. Hadjiantoniou, J. L. Harden, I. S. Skerjanc, and A. E. Pelling, Extracellular forces cause the nucleus to deform in a highly controlled anisotropic manner, Sci. Rep. **6**, 21300 (2016).

[3] R. Ungricht and U. Kutay, Mechanisms and functions of nuclear envelope remodelling, Nat. Rev. Mol. Cell Biol. **18**, 229 (2017).

[4] F.-Y. Chu, S. C. Haley, and A. Zidovska, On the origin of shape fluctuations of the cell nucleus, Proc. Natl. Acad. Sci. USA **114**, 10338 (2017).

[5] E. A. Rog-Zielinska, E. T. O'Toole, A. Hoenger, and P. Kohl, Mitochondrial deformation during the cardiac mechanical cycle, Anat. Rec. **302**, 146 (2019).

[6] Y. Kalukula, A. D. Stephens, J. Lammerding, and S. Gabriele, Mechanics and functional consequences of nuclear deformations, Nat. Rev. Mol. Cell Biol. **23**, 583 (2022).

[7] J. C. Del Alamo, G. N. Norwich, Y.-S. J. Li, J. C. Lasheras, and S. Chien, Anisotropic rheology and directional mechanotransduction in vascular endothelial cells, Proc. Natl. Acad. Sci. USA **105**, 15411 (2008).

[8] S. K. Gupta, Y. Li, and M. Guo, Anisotropic mechanics and dynamics of a living mammalian cytoplasm, Soft Matter **15**, 190 (2019).

[9] S. N. Hird and J. G. White, Cortical and cytoplasmic flow polarity in early embryonic cells of caenorhabditis elegans, J. Cell Biol. **121**, 1343 (1993).

[10] P. Khuc Trong, H. Doerflinger, J. Dunkel, D. St Johnston, and R. E. Goldstein, Cortical microtubule nucleation can organise the cytoskeleton of *Drosophila* oocytes to define the anteroposterior axis, Elife **4**, e06088 (2015).

[11] J. Prost, F. Jülicher, and J.-F. Joanny, Active gel physics, Nat. Phys. **11**, 111 (2015).

[12] A. Mogilner and A. Manhart, Intracellular fluid mechanics: Coupling cytoplasmic flow with active cytoskeletal gel, Annu. Rev. Fluid Mech. **50**, 347 (2018).

[13] V. E. Deneke, A. Puliafito, D. Krueger, A. V. Narla, A. De Simone, L. Primo, M. Vergassola, S. De Renzis, and S. Di Talia, Self-organized nuclear positioning synchronizes the cell cycle in *Drosophila* embryos, Cell **177**, 925 (2019).

[14] P. H. Htet and E. Lauga, Cortex-driven cytoplasmic flows in elongated cells: fluid mechanics and application to nuclear transport in *Drosophila* embryos, J. Roy. Soc. Interface **20**, 20230428 (2023).

[15] S. Dutta, R. Farhadifar, W. Lu, G. Kabacaoğlu, R. Blackwell, D. B. Stein, M. Lakonishok, V. I. Gelfand, S. Y. Shvartsman, and M. J. Shelley, Self-organized intracellular twisters, Nat. Phys. **20**, 666 (2024).

[16] N. M. Ramdas and G. Shivashankar, Cytoskeletal control of nuclear morphology and chromatin organization, J. Mol. Biol. **427**, 695 (2015).

[17] D. Saintillan, M. J. Shelley, and A. Zidovska, Extensile motor activity drives coherent motions in a model of interphase chromatin, Proc. Natl. Acad. Sci. USA **115**, 11442 (2018).

[18] A. D. Stephens, E. J. Banigan, and J. F. Marko, Chromatin's physical properties shape the nucleus and its functions, Curr. Opin. Cell Biol. **58**, 76 (2019).

[19] A. Zidovska, The self-stirred genome: large-scale chromatin dynamics, its biophysical origins and implications, Curr. Op. Genet. Dev. **61**, 83 (2020).

[20] C. J. Walker, C. Crocini, D. Ramirez, A. R. Killaars, J. C. Grim, B. A. Aguado, K. Clark, M. A. Allen, R. D. Dowell, L. A. Leinwand *et al.*, Nuclear mechanosensing drives chromatin remodelling in persistently activated fibroblasts, Nat. Biomed. Eng. **5**, 1485 (2021).

[21] M. J. Shelley, The dynamics of microtubule/motor-protein assemblies in biology and physics, Annu. Rev. Fluid Mech. **48**, 487 (2016).

[22] D. Oriola, D. J. Needleman, and J. Brugués, The physics of the metaphase spindle, Annu. Rev. Biophys. **47**, 655 (2018).

[23] D. Oriola, F. Jülicher, and J. Brugués, Active forces shape the metaphase spindle through a mechanical instability, Proc. Natl. Acad. Sci. USA **117**, 16154 (2020).
[24] B. Aigouy, R. Farhadifar, D. B. Staple, A. Sagner, J.-C. Röper, F. Jülicher, and S. Eaton, Cell flow reorients the axis of planar polarity in the wing epithelium of *Drosophila*, Cell **142**, 773 (2010).
[25] M. Murrell, P. W. Oakes, M. Lenz, and M. L. Gardel, Forcing cells into shape: the mechanics of actomyosin contractility, Nat. Rev. Mol. Cell. Biol. **16**, 486 (2015).
[26] A. Boutillon, S. P. Banavar, and O. Campàs, Conserved physical mechanisms of cell and tissue elongation, Development **151**, dev202687 (2024).
[27] I. I. Smalyukh, J. Butler, J. D. Shrout, M. R. Parsek, and G. C. Wong, Elasticity-mediated nematiclike bacterial organization in model extracellular DNA matrix, Phys. Rev. E **78**, 030701 (2008).
[28] H.-C. Flemming and J. Wingender, The biofilm matrix, Nat. Rev. Microbiol. **8**, 623 (2010).
[29] A. Sokolov and I. S. Aranson, Physical properties of collective motion in suspensions of bacteria, Phys. Rev. Lett. **109**, 248109 (2012).
[30] D. Saintillan, Rheology of active fluids, Annu. Rev. Fluid Mech. **50**, 563 (2018).
[31] S. E. Spagnolie and P. T. Underhill, Swimming in complex fluids, Annu. Rev. Condens. Mat. Phys. **14**, 381 (2023).
[32] F. Ndlec, T. Surrey, A. C. Maggs, and S. Leibler, Self-organization of microtubules and motors, Nature (London) **389**, 305 (1997).
[33] C. Dombrowski, L. Cisneros, S. Chatkaew, R. E. Goldstein, and J. O. Kessler, Self-concentration and large-scale coherence in bacterial dynamics, Phys. Rev. Lett. **93**, 098103 (2004).
[34] D. Saintillan and M. J. Shelley, Instabilities and pattern formation in active particle suspensions: kinetic theory and continuum simulations, Phys. Rev. Lett. **100**, 178103 (2008).
[35] T. Sanchez, D. T. Chen, S. J. DeCamp, M. Heymann, and Z. Dogic, Spontaneous motion in hierarchically assembled active matter, Nature (London) **491**, 431 (2012).
[36] A. Doostmohammadi, J. Ignés-Mullol, J. M. Yeomans, and F. Sagués, Active nematics, Nat. Commun. **9**, 3246 (2018).
[37] R. A. Simha and S. Ramaswamy, Hydrodynamic fluctuations and instabilities in ordered suspensions of self-propelled particles, Phys. Rev. Lett. **89**, 058101 (2002).
[38] G. Subramanian and D. L. Koch, Critical bacterial concentration for the onset of collective swimming, J. Fluid Mech. **632**, 359 (2009).
[39] S. Ramaswamy, The mechanics and statistics of active matter, Annu. Rev. Condens. Matter Phys. **1**, 323 (2010).
[40] C. Hohenegger and M. J. Shelley, Stability of active suspensions, Phys. Rev. E **81**, 046311 (2010).
[41] L. Giomi, L. Mahadevan, B. Chakraborty, and M. Hagan, Banding, excitability and chaos in active nematic suspensions, Nonlinearity **25**, 2245 (2012).
[42] S. P. Thampi, R. Golestanian, and J. M. Yeomans, Instabilities and topological defects in active nematics, Europhys. Lett. **105**, 18001 (2014).
[43] S. Weady, Variational bounds and nonlinear stability of an active nematic suspension, J. Fluid Mech. **988**, A5 (2024).
[44] L. Giomi, Geometry and topology of turbulence in active nematics, Phys. Rev. X **5**, 031003 (2015).
[45] L. Giomi, L. Mahadevan, B. Chakraborty, and M. F. Hagan, Excitable patterns in active nematics, Phys. Rev. Lett. **106**, 218101 (2011).
[46] J. Dunkel, S. Heidenreich, K. Drescher, H. H. Wensink, M. Bär, and R. E. Goldstein, Fluid dynamics of bacterial turbulence, Phys. Rev. Lett. **110**, 228102 (2013).
[47] L. Ohm and M. J. Shelley, Weakly nonlinear analysis of pattern formation in active suspensions, J. Fluid Mech. **942**, A53 (2022).
[48] A. J. Tan, E. Roberts, S. A. Smith, U. A. Olvera, J. Arteaga, S. Fortini, K. A. Mitchell, and L. S. Hirst, Topological chaos in active nematics, Nat. Phys. **15**, 1033 (2019).
[49] F. L. Memarian, D. Hammar, M. M. H. Sabbir, M. Elias, K. A. Mitchell, and L. S. Hirst, Controlling chaos: Periodic defect braiding in active nematics confined to a cardioid, Phys. Rev. Lett. **132**, 228301 (2024).
[50] M. Theillard, R. Alonso-Matilla, and D. Saintillan, Geometric control of active collective motion, Soft Matter **13**, 363 (2017).
[51] C. Joshi, Z. Zarei, M. M. Norton, S. Fraden, A. Baskaran, and M. F. Hagan, From disks to channels: dynamics of active nematics confined to an annulus, Soft Matter **19**, 5630 (2023).
[52] F. C. Keber, E. Loiseau, T. Sanchez, S. J. DeCamp, L. Giomi, M. J. Bowick, M. C. Marchetti, Z. Dogic, and A. R. Bausch, Topology and dynamics of active nematic vesicles, Science **345**, 1135 (2014).
[53] J. Brugués and D. Needleman, Physical basis of spindle self-organization, Proc. Natl. Acad. Sci. USA **111**, 18496 (2014).
[54] R. Zhang, Y. Zhou, M. Rahimi, and J. J. De Pablo, Dynamic structure of active nematic shells, Nat. Commun. **7**, 13483 (2016).
[55] M. Leoni, O. V. Manyuhina, M. J. Bowick, and M. C. Marchetti, Defect driven shapes in nematic droplets: analogies with cell division, Soft Matter **13**, 1257 (2017).
[56] H. Soni, W. Luo, R. A. Pelcovits, and T. R. Powers, Stability of the interface of an isotropic active fluid, Soft Matter **15**, 6318 (2019).
[57] R. Alert, Fingering instability of active nematic droplets, J. Phys. A **55**, 234009 (2022).
[58] G. Livne, S. Gat, S. Armon, and A. Bernheim-Groswasser, Self-assembled active actomyosin gels spontaneously curve and wrinkle similar to biological cells and tissues, Proc. Natl. Acad. Sci. USA **121**, e2309125121 (2024).
[59] M. Firouznia and D. Saintillan, Self-organized dynamics of a viscous drop with interfacial nematic activity, Phys. Rev. Res. **7**, L012054 (2025).
[60] A. Mogilner and G. Oster, Cell motility driven by actin polymerization, Biophys. J. **71**, 3030 (1996).
[61] T. Svitkina, The actin cytoskeleton and actin-based motility, Cold Spring Harb. Perspect. Biol. **10**, a018267 (2018).
[62] C. C. Maass, C. Krüger, S. Herminghaus, and C. Bahr, Swimming droplets, Annu. Rev. Condens. Matter Phys. **7**, 171 (2016).
[63] T. Gao and Z. Li, Self-driven droplet powered by active nematics, Phys. Rev. Lett. **119**, 108002 (2017).
[64] X. Wang, R. Zhang, A. Mozaffari, J. J. de Pablo, and N. L. Abbott, Active motion of multiphase oil droplets: emergent dynamics of squirmers with evolving internal structure, Soft Matter **17**, 2985 (2021).

[65] Y.-N. Young, M. Shelley, and D. Stein, The many behaviors of deformable active droplets, Math. Biosci. Eng. **18**, 2849 (2021).

[66] H. Stark, Physics of colloidal dispersions in nematic liquid crystals, Phys. Rep. **351**, 387 (2001).

[67] I. Musevic, *Liquid Crystal Colloids* (Springer, Cham, Switzerland, 2017).

[68] I. I. Smalyukh, Liquid crystal colloids, Annu. Rev. Condens. Mat. Phys. **9**, 207 (2018).

[69] K. Nayani, A. A. Evans, S. E. Spagnolie, and N. L. Abbott, Dynamic and reversible shape response of red blood cells in synthetic liquid crystals, Proc. Natl. Acad. Sci. USA **117**, 26083 (2020).

[70] H. Ghaiedi, L. C. P. Herrera, S. Alshafeay, L. Harris, J. Almodovar, and K. Nayani, Liquid crystalline collagen assemblies as substrates for directed alignment of human Schwann cells, Soft Matter **20**, 8997 (2024).

[71] S. Ray, J. Zhang, and Z. Dogic, Rectified rotational dynamics of mobile inclusions in two-dimensional active nematics, Phys. Rev. Lett. **130**, 238301 (2023).

[72] A. J. H. Houston and G. P. Alexander, Colloids in two-dimensional active nematics: conformal cogs and controllable spontaneous rotation, New J. Phys. **25**, 123006 (2023).

[73] C. Singh and A. Chaudhuri, Anomalous dynamics of a passive droplet in active turbulence, Nat. Commun. **15**, 3704 (2024).

[74] G. Negro, L. C. Head, L. N. Carenza, T. N. Shendruk, D. Marenduzzo, G. Gonnella, and A. Tiribocchi, Topology controls flow patterns in active double emulsions, Nat. Commun. **16**, 1412 (2025).

[75] J. B. Freund, Object transport by a confined active suspension, J. Fluid Mech. **960**, A16 (2023).

[76] L. D. Landau, E. M. Lifshitz, A. M. Kosevich, and L. P. Pitaevskii, *Theory of Elasticity* (Elsevier, Oxford, UK – (Butterworth-Heinemann), 1986), Vol. 7.

[77] P.-G. De Gennes and J. Prost, *The Physics of Liquid Crystals* (Oxford University Press, Oxford, UK, 1993).

[78] I. W. Stewart, *The Static and Dynamic Continuum Theory of Liquid Crystals: A Mathematical Introduction* (CRC Press, Boca Raton, FL, 2004).

[79] M. C. Marchetti, J. F. Joanny, S. Ramaswamy, T. B. Liverpool, J. Prost, M. Rao, and R. A. Simha, Hydrodynamics of soft active matter, Rev. Mod. Phys. **85**, 1143 (2013).

[80] T. G. J. Chandler and S. E. Spagnolie, Rigid and deformable bodies in nematic liquid crystals, Phys. Rev. Fluids **9**, 110511 (2024).

[81] D. Saintillan and M. J. Shelley, Theory of active suspensions, in *Complex Fluids in Biological Systems* (Springer, New York, NY, 2015), pp. 319–351.

[82] See Supplemental Material at http://link.aps.org/supplemental/10.1103/x8y2-tw4c for further mathematical details.

[83] A. Rapini and M. Papoular, Distorsion d'une lamelle nématique sous champ magnétique conditions d'ancrage aux parois, J. Phys. Colloq. **30**, C4-54 (1969).

[84] M. J. Ablowitz, A. S. Fokas, and A. S. Fokas, *Complex Variables: Introduction and Applications* (Cambridge University Press, Cambridge, UK, 2003).

[85] H. Miyazako and T. Nara, Explicit calculation method for cell alignment in non-circular geometries, R. Soc. Open Sci. **9**, 211663 (2022).

[86] H. Miyazako and T. Sakajo, Defect pairs in nematic cell alignment on doubly connected domains, Proc. R. Soc. A. **480**, 20230879 (2024).

[87] W. E. Langlois and M. O. Deville, *Slow Viscous Flow* (Springer, Cham, Switzerland, 1964).

[88] T. G. J. Chandler and S. E. Spagnolie, A nematic liquid crystal with an immersed body: equilibrium, stress, and paradox, J. Fluid Mech. **967**, A19 (2023).

[89] T. G. J. Chandler and S. E. Spagnolie, Exact and approximate solutions for elastic interactions in a nematic liquid crystal, SIAM J. Appl. Math. **84**, 2476 (2024).

[90] A. H. England, *Complex Variable Methods in Elasticity* (Wiley-lnterscience, New York, NY, 1971).

[91] P. Howell, G. Kozyreff, and J. Ockendon, *Applied Solid Mechanics* (Cambridge University Press, Cambridge, UK, 2009), Vol. 43.

[92] G. E. Volovik and O. D. Lavrentovich, Topological dynamics of defects: boojums in nematic drops, Zh. Eksp. Teor. Fiz. **85**, 1997 (1983).

[93] R. E. Goldstein, I. Tuval, and J.-W. van de Meent, Microfluidics of cytoplasmic streaming and its implications for intracellular transport, Proc. Natl. Acad. Sci. USA **105**, 3663 (2008).

[94] N. Fakhri, A. D. Wessel, C. Willms, M. Pasquali, D. R. Klopfenstein, F. C. MacKintosh, and C. F. Schmidt, High-resolution mapping of intracellular fluctuations using carbon nanotubes, Science **344**, 1031 (2014).

[95] E. F. Koslover, C. K. Chan, and J. A. Theriot, Cytoplasmic flow and mixing due to deformation of motile cells, Biophys. J. **113**, 2077 (2017).

[96] S. S. Mogre, A. I. Brown, and E. F. Koslover, Getting around the cell: physical transport in the intracellular world, Phys. Biol. **17**, 061003 (2020).

[97] C. D. Schimming and J. Viñals, Equilibrium morphology of tactoids in elastically anisotropic nematics, Soft Matter **18**, 8024 (2022).

[98] E. Villermaux, Mixing versus stirring, Annu. Rev. Fluid Mech. **51**, 245 (2019).

[99] E. Gouillart, N. Kuncio, O. Dauchot, B. Dubrulle, S. Roux, and J.-L. Thiffeault, Walls inhibit chaotic mixing, Phys. Rev. Lett. **99**, 114501 (2007).

[100] E. Tjhung, D. Marenduzzo, and M. E. Cates, Spontaneous symmetry breaking in active droplets provides a generic route to motility, Proc. Natl. Acad. Sci. USA **109**, 12381 (2012).

[101] L. Giomi and A. DeSimone, Spontaneous division and motility in active nematic droplets, Phys. Rev. Lett. **112**, 147802 (2014).

[102] G. Kokot, H. A. Faizi, G. E. Pradillo, A. Snezhko, and P. M. Vlahovska, Spontaneous self-propulsion and nonequilibrium shape fluctuations of a droplet enclosing active particles, Commun. Phys. **5**, 91 (2022).

[103] A. Desai, A. Murray, T. J. Mitchison, and C. E. Walczak, The use of *Xenopus* egg extracts to study mitotic spindle assembly and function *in vitro*, Meth. Cell Biol. **61**, 385 (1998).

[104] Y. Shimamoto, Y. T. Maeda, S. Ishiwata, A. J. Libchaber, and T. M. Kapoor, Insights into the micromechanical properties of the metaphase spindle, Cell **145**, 1062 (2011).

[105] G. C. Rogers, S. L. Rogers, T. A. Schwimmer, S. C. Ems-McClung, C. E. Walczak, R. D. Vale, J. M. Scholey, and

D. J. Sharp, Two mitotic kinesins cooperate to drive sister chromatid separation during anaphase, Nature (London) **427**, 364 (2004).

[106] C.-H. Yu, S. Redemann, H.-Y. Wu, R. Kiewisz, T. Y. Yoo, W. Conway, R. Farhadifar, T. Müller-Reichert, and D. Needleman, Central-spindle microtubules are strongly coupled to chromosomes during both anaphase A and anaphase B, Mol. Biol. Cell **30**, 2503 (2019).

[107] C. P. Kelleher, Y. P. Rana, and D. J. Needleman, Long-range repulsion between chromosomes in mammalian oocyte spindles, Sci. Adv. **10**, eadq7540 (2024).

[108] S. P. Thampi, R. Golestanian, and J. M. Yeomans, Velocity correlations in an active nematic, Phys. Rev. Lett. **111**, 118101 (2013).

[109] A. D. Rey, Liquid crystal models of biological materials and processes, Soft Matter **6**, 3402 (2010).